

## *Bach2* Deficiency Promotes Intestinal Epithelial Regeneration by Accelerating DNA Repair in Intestinal Stem Cells

Yuanchuang Li,<sup>1,6</sup> Xinxin Rao,<sup>1,6</sup> Peiyuan Tang,<sup>1</sup> Shengzhi Chen,<sup>1</sup> Qiang Guo,<sup>1</sup> Guoxiang Fu,<sup>1</sup> Mengxue Pan,<sup>1</sup> Liping Liang,<sup>2</sup> Ye Yao,<sup>2</sup> Xiaoxue Gao,<sup>1</sup> Yi Zhou,<sup>1</sup> Zhen Zhang,<sup>2</sup> Xiaoya Xu,<sup>1</sup> Wenhao Hu,<sup>3,4</sup> Jianjun Gao,<sup>1,\*</sup> and Guoqiang Hua<sup>1,5,\*</sup>

<sup>1</sup>Institute of Radiation Medicine, Fudan University, 2094 Xietu Road, Shanghai 200032, China

<sup>2</sup>Department of Radiation Oncology, Fudan University Shanghai Cancer Center, Fudan University, 270 Dong'an Road, Shanghai 200032, China

<sup>3</sup>Human Oncology and Pathogenesis Program, Memorial Sloan Kettering Cancer Center, New York, NY 10065, USA

<sup>4</sup>Marie-Josée and Henry R. Kravis Center for Molecular Oncology, Memorial Sloan Kettering Cancer Center, New York, NY 10065, USA

<sup>5</sup>Cancer Institute, Fudan University Shanghai Cancer Center, Fudan University, Shanghai 200032, China

<sup>6</sup>Co-first author

\*Correspondence: [jjgao@shmu.edu.cn](mailto:jjgao@shmu.edu.cn) (J.G.), [guoqianghua@fudan.edu.cn](mailto:guoqianghua@fudan.edu.cn) (G.H.)

<https://doi.org/10.1016/j.stemcr.2020.12.005>

### SUMMARY

Epithelial regeneration is critical for barrier maintenance and organ function after intestinal injury, although the repair mechanisms are unclear. Here, we found that *Bach2* deficiency promotes intestinal epithelial cell proliferation during homeostasis. Moreover, genetic inactivation of *Bach2* in mouse intestinal epithelium facilitated crypt regeneration after irradiation, resulting in a reduction in mortality. RNA-sequencing analysis of isolated crypts revealed that *Bach2* deficiency altered the expression of numerous genes, including those regulating double-strand break repair. Mechanistic characterizations indicated that *Bach2* deletion facilitated DNA repair in intestinal crypt cells, as evidenced by faster resolution of  $\gamma$ -H2AX and 53BP1 foci in *Bach2*<sup>-/-</sup> crypt cells, compared with *Bach2*<sup>+/+</sup> control. Together, our studies highlight that *Bach2* deficiency promotes intestinal regeneration by accelerating DNA repair in intestinal stem cells after radiation damage.

### INTRODUCTION

The mammalian intestinal epithelium is well suited to the study of tissue regeneration, as it has a constitutively high rate of cell turnover (every 3–5 days) and a well-delineated stem/progenitor cell hierarchy (Bjerknes and Cheng, 1999). The rapid turnover of gastrointestinal (GI) mucosa is driven by the mitotic activity of its stem cells characterized by expression of the *Wnt* target gene *Lgr5* (leucine-rich-repeat-containing G-protein-coupled receptor 5, also known as *Gpr49*) (Barker et al., 2007). Acute exposure to a high dose of ionizing radiation (IR) can damage GI mucosa and cause diffuse inflammation of the GI tract (Waselenko et al., 2004). Mice exposed to higher doses of radiation die within 10 days owing to disruption in the small intestine epithelium (Mason et al., 1989; Terry and Travis, 1989). The pathophysiology of lethal GI tract damage involves depletion of the pool of stem cells residing at the bottom of the crypts of Lieberkühn, which impairs the regeneration of villus/crypt units and compromises the mucosal integrity and function. Although several countermeasures already have FDA investigational new drug status (CBLB-502, 5-AED, Bio300, EX-Rad) and other promising mitigators are in development, there are still no FDA-approved effective countermeasures for the GI syndrome (Singh et al., 2012) at present. Novel therapeutic principles targeting tissue regeneration are urgently needed to treat the radiation-induced GI syndrome.

Intestinal stem cells (ISCs), also called crypt-based columnar cells (CBCs), were reported to be responsible for intestinal regeneration after radiation damage (Hua et al., 2012). Accumulating evidence shows that stem cells are endowed with a superior capacity to prevent the accumulation of genetic lesions and repair them (Vitale et al., 2017). Sotiropoulou et al. reported that hair-follicle-bulge stem cells are relatively radioresistant due to the higher expression of the antiapoptotic gene *Bcl-2* and transient stabilization of P53 after DNA damage (Panagiota A et al., 2010). Hua et al. reported that ISCs repair DNA double-strand breaks (DSBs) more efficiently than differentiated GI cells (Hua et al., 2012). Hematopoietic stem cells (HSCs) use multiple mechanisms to prevent the accrual of mutations or their transmission to the progeny, and baseline DNA repair is highly efficient in HSCs (Vitale et al., 2017). Genetic lesions are especially detrimental to stem cell maintenance and tissue regeneration, providing the rationale for the development of specific therapeutic strategies.

Recent published data have implicated that *Bach2* (BTB and CNC homology 2) is important in the maintenance of tissue immune homeostasis (Roychoudhuri et al., 2013; Srividya et al., 2013) and plays a vital role in regulating the cell cycle and DNA repair (Uittenboogaard et al., 2013). As an important transcription factor, *Bach2* was primarily reported to induce apoptosis via inhibition of the NRF2-mediated antioxidant defense pathway



(Akihiko et al., 2014; Hoshino et al., 2000; Muto et al., 1998; Oyake et al., 1996). Genetic silencing of *Bach2* stimulates proliferation and increases cell survival in response to acute oxidative stress according to an experiment performed on NIH3T3 fibroblasts (Uittenboogaard et al., 2013). In addition, it has been verified that *Bach2* can induce *p53* expression during early B cell development (Srividya et al., 2013) and was required for efficient formation of regulatory T cells and suppression of lethal inflammation (Roychoudhuri et al., 2013). Importantly, *Bach2*-deficient mice exhibit a hypertrophic crypts phenotype in the small intestinal epithelium at 3 months of age and develop a progressive wasting disease, resulting in diminished survival compared with wild-type (WT) control mice, within 300 days (Roychoudhuri et al., 2013). These studies suggest that *Bach2* may play a key role in determining cell cycle; however, the detailed functional role of *Bach2* in intestinal regeneration and DNA damage responses after radiation is still ambiguous. Here, using *Bach2*-knockout (KO) mice and an intestinal organoid-based functional model, we found that *Bach2* represents a key regulator of intestinal regeneration by facilitating DNA repair after radiation.

## RESULTS

### *Bach2* Deficiency Promotes Intestinal Epithelial Cell Proliferation

Initially, we investigated *Bach2* expression in intestinal crypts isolated from *Lgr5*-EGFP transgenic mice, confirming a higher expression level in *Lgr5*<sup>+</sup> ISCs than in *Lgr5*<sup>-</sup> transient amplifying (TA) cells (Figure 1A). To further investigate whether the protein level of *Bach2* is also enriched in ISCs, immunohistochemistry (IHC) staining of BACH2 was performed. We generated *Bach2*<sup>fl/fl</sup>; *CreER*<sup>T2</sup> mice by crossing *Bach2*-floxed mice with *CreER*<sup>T2</sup> mice. *Bach2* conditional KO was achieved through tamoxifen (Tam) administration and its deletion was confirmed by western blot analysis as well as real-time qPCR in intestinal epithelial and spleen (Figure S1A and S1B). *Bach2* is highly expressed in the immune system, which is essential for development of T and B lymphocytes. To exclude the possible impact of alterations in immune function, we further generated *Bach2* intestinal-specific-KO (*Bach2*<sup>fl/fl</sup>; *Villin-CreER*<sup>T2</sup>, vKO) mice using *Villin-CreER*<sup>T2</sup> mice to explore the role of *Bach2* locally (Figure 1B). Figure 1C and 1D shows that BACH2<sup>+</sup> cells are concentrated in the region of CBCs. We found that 75.48 ± 3.63% of CBCs and 15.45 ± 2.72% of TA cells in WT mice are BACH2-positive cells. This indicates that *Bach2* may play a unique role in regulating ISC functions. Moreover, we next studied the changes in *Bach2* expression following 12 Gy irradiation. Our IHC data show that there is no significant change in BACH2 expres-

sion during the first 24 h after irradiation, whereas a dramatic increase in BACH2 expression was observed in regenerating crypts (84 h after IR) (Figures S1C and S1D).

We speculate that *Bach2* deficiency may lead to abnormal phenotype in mouse intestinal epithelium. Indeed, *Bach2*-KO and vKO mice show enlarged intestinal crypts compared with WT controls at 3 months after Tam injection (Figure 1E). The average depth of crypts of control mice was 52.57 ± 1.54 μm, while the average depth of crypts was 74.92 ± 1.71 μm (*p* < 0.001) and 76.06 ± 1.74 μm (*p* < 0.001) from *Bach2*-KO and vKO groups, respectively (Figure 1F). Similarly, the average length of villus of control mice was significantly shorter than those of *Bach2*-KO (*p* < 0.001) and vKO (*p* < 0.001) groups, respectively (Figure 1G). In addition, 5-ethynyl-2'-deoxyuridine (EdU) incorporation assay was performed to further explore the effect of *Bach2* deficiency on cell proliferation. Likewise, our results show that the proportion of EdU<sup>+</sup> cells in crypts of KO mice is much higher than that in WT control (14.74 ± 0.36 EdU<sup>+</sup> cells/*Bach2*-KO crypt versus 7.68 ± 0.34 EdU<sup>+</sup> cells/control crypt, *p* < 0.001) (Figures 1H and 1I). To investigate the effect of *Bach2* deficiency on cell apoptosis, cleaved caspase-3 IHC staining was conducted. Our data show that there was no significant difference in apoptosis rates in the crypt cells between *Bach2*-KO mice and WT controls during homeostasis and the early phase after irradiation (Figure S2).

*Bach2* deficiency promotes the proliferation of intestinal epithelium; thus, we asked whether *Bach2* ablation could also regulate ISC homeostasis and self-renewal. To test this hypothesis, the expression of a set of stem cell-related genes, including *Olfm4*, *CD44*, *Sox9*, *Lgr5*, and *Lysozyme*, was assessed. Figure 1J shows that there were significant changes in the expression of intestinal progenitor cell markers (CD44 and SOX9), whereas no significant changes were found in the expression of ISC markers (LGR5 and OLFM4) or Paneth cell marker (LYSOZYME). These immune-staining data were validated by real-time qPCR (Figure 1K). These results suggested that *Bach2* ablation in the small intestinal epithelia has no influence on ISC numbers, but promotes the proliferation of intestinal progenitor cells.

### *Bach2* Ablation Promotes Intestinal Organoid Growth

To confirm the increased proliferation in the crypt epithelial compartment is a result of abnormal alteration in epithelial cells, *ex vivo* organoid formation assay was performed. Small intestinal crypts isolated from *Bach2*-KO (or *Bach2*-vKO) and *Bach2*-floxed control mice (or *Villin-CreER*<sup>T2</sup>, *Villin-Cre*) were embedded in 3D Matrigel. 4-Hydroxytamoxifen (100 nM) was added to the culture medium to induce CreER activation or to remove floxed *Bach2* alleles (Schwank and Clevers, 2016). Under this

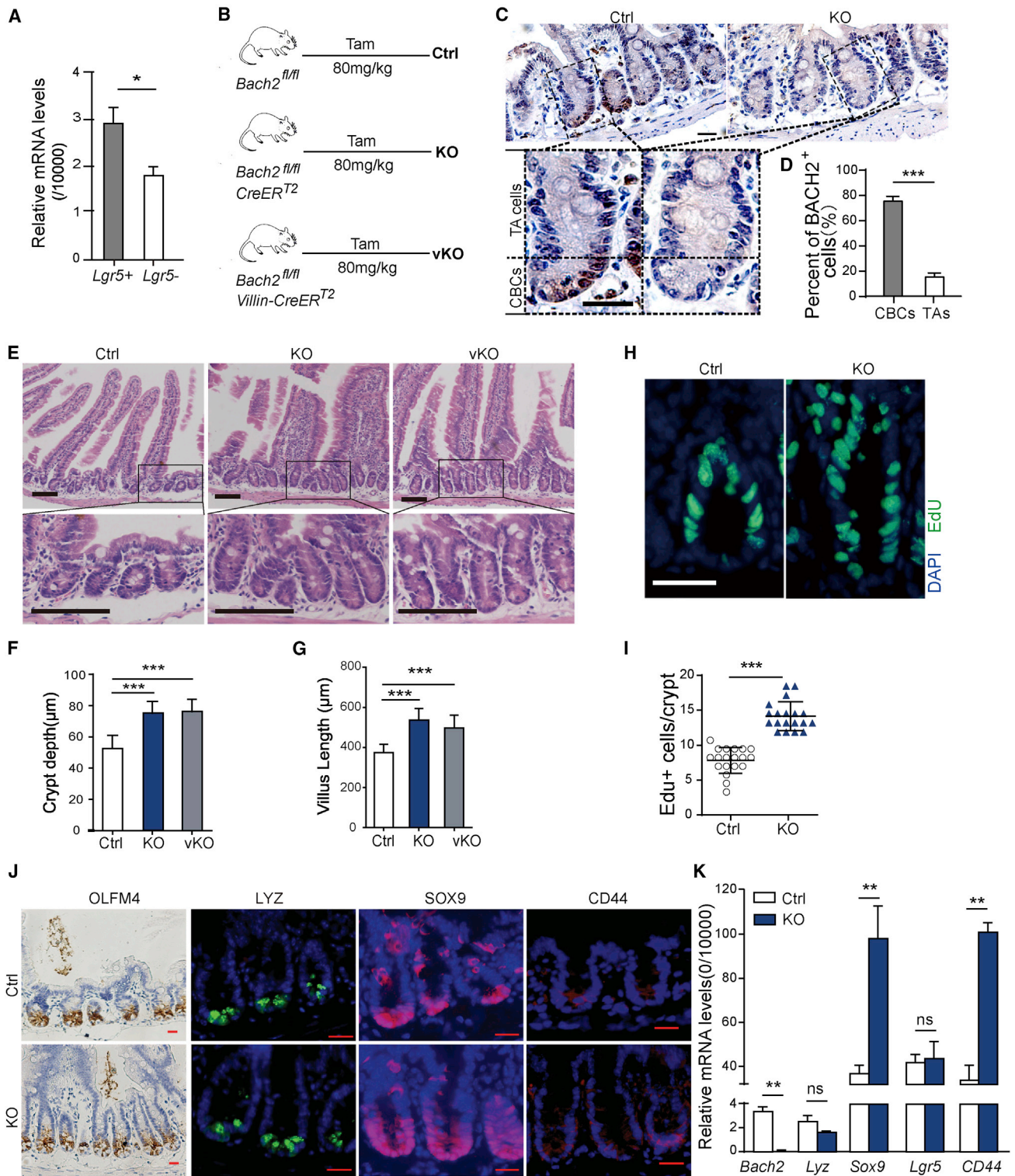


**Figure 1. *Bach2* Ablation Promotes Intestinal Epithelial Cell Proliferation In Vivo**

(A) LGR5<sup>+</sup> intestinal stem cells (ISCs) and LGR5<sup>-</sup> transient amplifying (TA) cells obtained by cell sorting from crypt cells of *Lgr5-EGFP* transgenic mice. *Bach2* was expressed in crypt cells, with a higher level in ISCs than in TA cells, as determined by real-time PCR (n = 6 mice). (B) Schematic diagram of Tam administration in *Bach2* conditional knockout mice (globally [KO] or intestinal epithelial cell specifically [vKO]).

(legend continued on next page)



dosage of Tam, no significant defect appeared in *Villin-Cre* organoids compared with WT, indicating no harmful impact of CreER activation alone *in vitro* (Figures S3A and S3B). After induction, the *Bach2* mRNA expression level was further examined by real-time qPCR (Figure S3C). On day 6 of culture, we observed an obvious increase in organoid size and bud numbers of organoids derived from *Bach2*-KO or *Bach2*-vKO mice compared with *Bach2*-floxed controls (Figure 2A). Bud formation efficiency represents organoid growth ability. Nearly 80% of *Bach2*-deficient organoids had at least three buds, while only 60% of *Bach2*-floxed (control, Ctrl) organoids had three buds (Figure 2B). By calculating, we showed that the average projected surface area of *Bach2*-deficient organoids was significantly larger than that of controls (20,572 ± 727.3 and 15,830 ± 702.0 pixels, respectively,  $p < 0.001$ ) (Figure 2C). Correspondingly, the expression levels of key proliferation and differentiation markers were measured by qPCR (Figure 2D). Organoid data are consistent with the results from *in vivo* analysis. The expression levels of *CD44* and *Sox9* in *Bach2*-KO organoids were increased compared with control organoids, while no significant difference was found in the expression of *Lgr5* (Figure 2D).

### ***Bach2* Deficiency Promotes the Regeneration of Intestinal Crypts *In Vivo***

*Bach2* silencing had been reported to increase cell viability after exposure to toxic levels of oxidative stress (Uittenboogaard et al., 2013). In this study, we intended to investigate whether *Bach2* ablation can protect intestinal crypt against acute radiation exposure. A microcolony assay was conducted to investigate the regeneration capacity of ISCs on day 3.5 after 12 Gy subtotal body irradiation (SBI). Mice were injected intraperitoneally with Tam (80 mg/kg) for 5 consecutive days and 12 Gy radiation was given on day 10 after the last Tam injection (illustrated in Figure 3A). Our data show that the ISC impairment by CreER toxicity returned to normal by 9 days post Tam, which is consistent with published data (Figures S4A–S4C) (Bohin et al., 2018). At 3.5 days after irradiation, *Bach2*-floxed

control mice contained 21 ± 6 crypts, while *Bach2*-KO mice had 63 ± 15 crypts ( $p < 0.001$ ) (Figures 3B and 3C). We further measured the projected surface areas of the regenerated crypts in two groups, and found obvious increases in the size of regenerating crypts from *Bach2*-KO mice (Figure 3D). Ki67 immunostaining also exhibited a clear difference between *Bach2*-deficient crypts and control ones, suggesting that *Bach2* ablation indeed promotes intestinal crypt regeneration after high doses of radiation (Figures 3E and 3F).

Given the possible impact of alteration in immune function, we further asked whether intestinal epithelial cell-specific deletion of *Bach2* (vKO, *Bach2<sup>fl/fl</sup>*; *Villin-CreER<sup>T2</sup>*) enhances intestinal crypt regeneration. As was expected, on day 3.5 post IR, the number of regenerating crypts in the small intestine of vKO mice also significantly increased, nearly 2.3-fold more than that of control (Figures 4A and 4B). The projected surface area of the regenerated crypts and the number of Ki67<sup>+</sup> crypt cells were also correspondently increased in vKO mice compared with control group (Figures 4C–4E). These data indicated that *Bach2* deletion, either globally or locally, indeed promotes intestinal crypt regeneration after radiation damage.

### ***Bach2* Ablation Promotes Organoid Regeneration *In Vitro***

The ISCs are major cells responsible for epithelial regeneration. To confirm the direct role of *Bach2* in the regeneration of ISCs, we performed *in vitro* organoid formation assay in 3D cultures. Intestinal crypts were isolated from small intestine of *Bach2*-KO and *Bach2*-floxed control mice (Ctrl) or from *Villin-CreER<sup>T2</sup>* mice (*Villin-Cre*). 4-Hydroxytamoxifen was added to induce CreER activation and/or *Bach2* deletion, and 6 Gy X-ray radiation was performed 1 day later. *Bach2* deletion was regularly checked by real-time qPCR analysis. Consistent with the *in vivo* data of *Bach2*-KO mice, *Bach2* ablation increased the organoid survival and the size of regenerating crypts (Figure 5A). On day 12 of culture, the percentage of surviving organoids from the KO group was 33% more than that of

(C) Representative images of *Bach2* IHC staining (dark brown) in intestinal crypts from *Bach2*-KO and WT mice 10 days after tamoxifen administration. Scale bars, 20 μm.

(D) Quantitative analysis of BACH2-positive cells in crypts from WT mice as examined by IHC study (n = 3 mice, mean ± SEM).

(E) H&E staining of small intestines with hypertrophic villus and crypts from *Bach2*-KO and vKO mice 3 months after *Bach2* ablation. Scale bars, 100 μm.

(F and G) Quantification of crypt depth (F) and villus length (G) from *Bach2*-KO, vKO, and control mice (n = 6 mice).

(H) Representative images of EdU immunofluorescence staining of intestinal crypts of *Bach2*-KO and Ctrl mice. Scale bar, 20 μm.

(I) Quantitative analysis of EdU<sup>+</sup> cells per crypt in *Bach2*-KO and Ctrl mice (n = 6 mice).

(J) IHC staining of intestinal stem cell marker OLFM4 and immunofluorescent staining of LYSOZYME, SOX9, and CD44. Scale bars, 20 μm.

(K) Quantitative real-time PCR analysis of stem cell-related gene expression in *Bach2*-KO and control crypts (n = 6 mice). Error bars, SD. \* $p < 0.05$ , \*\* $p < 0.01$ , \*\*\* $p < 0.001$ ; ns, no significance.

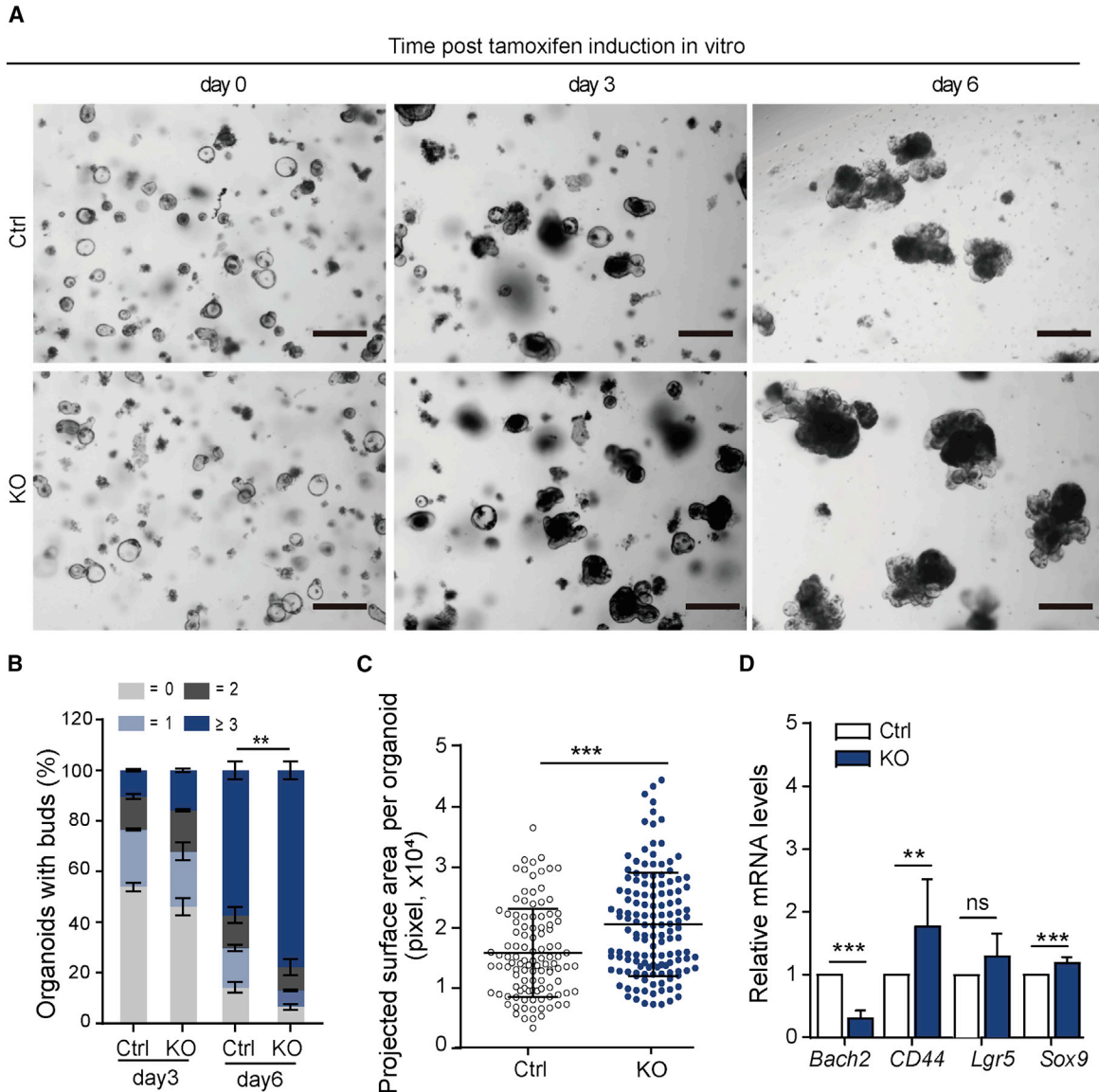


### Figure 2. *Bach2* Ablation Promotes Organoid Growth *In Vitro*

(A) Representative images of 3D organoid culture are shown from Ctrl and *Bach2*-KO mice. Crypts were isolated from *Bach2<sup>fl/fl</sup>* and *Bach2<sup>fl/fl</sup>; CreER<sup>T2</sup>* (or *Bach2<sup>fl/fl</sup>; Villin-CreER<sup>T2</sup>*) mice and embedded in Matrigel for organoid growth. 4-Hydroxytamoxifen (100 nM) was added to the culture medium to induce *Bach2* ablation. Scale bars, 200  $\mu$ m.

(B) Bud numbers were ascertained in 3D organoids ( $n > 80$  organoids per mouse; three mice per genotype). Bars show mean percentage of organoids with different bud numbers. Dark blue,  $\geq 3$ ; dark gray, 2; light blue, 1; light gray, 0.

(C) Organoid projected surface area is shown from Ctrl or KO mice ( $n > 100$  organoids from three mice per genotype).

(D) Quantitative real-time PCR analysis of stem cell-related gene expression in *Bach2*-KO and control mice-derived organoids ( $n = 6$  mice). Error bars, SD. \*\* $p < 0.01$ , \*\*\* $p < 0.001$ ; ns, no significance.

*Bach2*-floxed control (Ctrl), or 35% more than the *Villin-CreER<sup>T2</sup>* control (*Villin-Cre*) (Figure 5B). Meanwhile, the projected surface area of regenerating organoids was significantly larger than that of controls (Figure 5C). Moreover, we evaluated organoid viability using the CellTiter-Glo cell viability assay. The results obtained by using

the image-based organoid survival method and CellTiter-Glo cell viability assay have good consistency (Figure 5D). Together, these findings suggest that *Bach2* ablation directly enhances ISC radioresistance and increases cell viability after a high dose of irradiation, resulting in improved intestinal organoid survival.

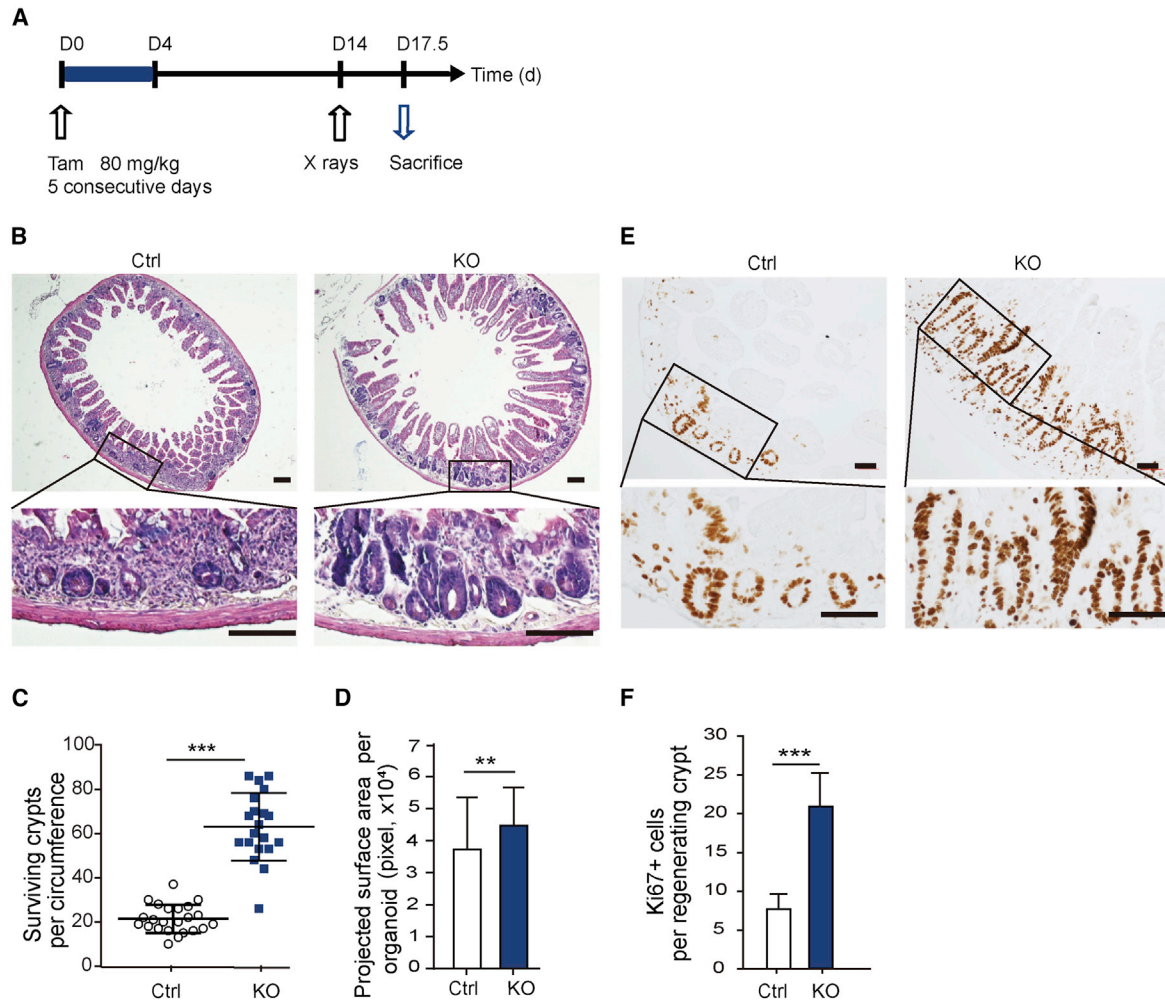


### Figure 3. *Bach2* Deficiency Promotes the Regeneration of Intestinal Crypts after Radiation Damage

(A) Experimental procedure: *Bach2* deletion was induced with 80 mg/kg tamoxifen for 5 consecutive days in mice (6–8 weeks of age), followed by a single dose of 12 Gy X-ray exposure at day 14, and the mice were sacrificed 3.5 days later for further processing.

(B) Representative full transverse sections of H&E staining of proximal jejunum from *Bach2*-KO and control mice at day 3.5 post irradiation. Scale bars, 200  $\mu$ m.

(C and D) Quantification of surviving crypts (C) and their size (D) at day 3.5 post irradiation as determined by crypt microcolony assay ( $n > 20$  crypts per group).

(E) Representative images of Ki-67 IHC staining (dark brown) in regenerated crypts from KO and control mice. Scale bars, 50  $\mu$ m.

(F) Quantitative analysis of Ki-67-positive cells as examined by IHC study ( $n > 20$  crypts per group).

Error bars, SD. \*\* $p < 0.01$ , \*\*\* $p < 0.001$ .

### *Bach2* Deletion Protects Mice from Radiation-Induced Mortality

We then asked whether *Bach2* deficiency has an impact on animal survival. A single dose of 14 Gy SBI induces GI syndrome and mortality of animals post exposure, verified by the autopsy results showing total or near-total depletion of the crypt compartment without extensive matrix necrosis in bone marrow. Animal survival was evaluated by Kaplan-Meier analysis. With a single dose of 14 Gy, nearly 89% of *Bach2*-KO mice continued to survive beyond

90 days (Figure 6A), and 80% of *Bach2*-vKO survived, compared with 40% of WT mice. Differences in the degree of small intestinal epithelial injury were evaluated by histological analysis on day 3.5 post IR (Figures S5A and S5B). A reduction in villus length and a complete destruction of the intestinal mucosa were observed in dying mice after 14 Gy X-ray irradiation (Figure 6B). Bone marrow analysis showed no obvious difference among groups, indicating that mice may die from radiation-induced GI syndrome (Figure 6B). We also monitored the dynamic weight changes in mice

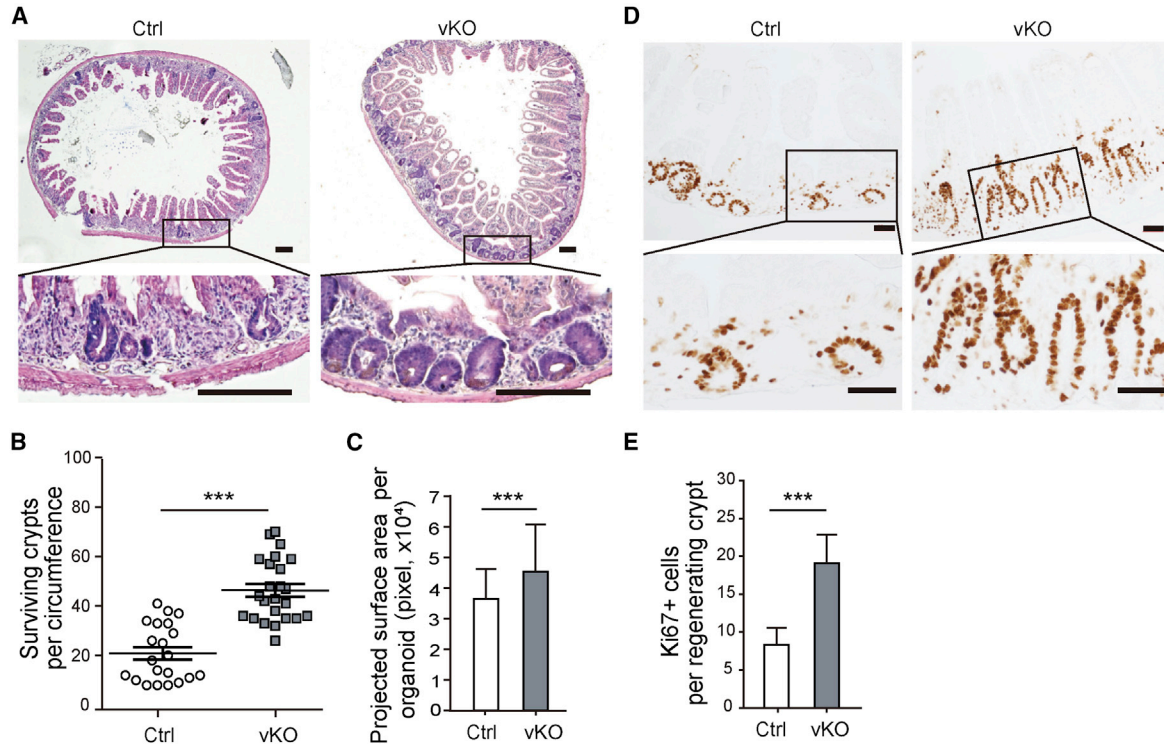


**Figure 4. Specific *Bach2* Ablation in Intestinal Epithelium Enhances Crypt Regeneration after Radiation Damage**

(A) Representative pictures of H&E staining of proximal jejunum from *Bach2* vKO and control mice at day 3.5 post irradiation. Scale bars, 200  $\mu$ m.

(B and C) Quantification of surviving crypts (B) and their size (C) at day 3.5 post irradiation as determined by crypt microcolony assay ( $n > 20$  crypts per group).

(D) Representative images of Ki-67 IHC staining (dark brown) in regenerated crypts from vKO and control mice. Scale bars, 50  $\mu$ m.

(E) Quantitative analysis of Ki-67-positive cells as examined by IHC study ( $n > 20$  crypts per group).

Error bars, SD. \*\*\* $p < 0.001$ .

in different groups over 90 days (Figure 6C). During the first 6 days post irradiation, mice in the three groups showed a declining trend in body weight and bad appetite. Mice in the *Bach2*-KO and vKO groups started to gain weight from day 6, while mice in the controlled group showed a slower mitigation sign. Taken together, our results show that *Bach2* ablation can protect crypt cells from radiation damage, resulting in a reduction in mouse mortality.

### ***Bach2* Deficiency Facilitates DNA Repair in Intestinal Crypt Cells**

To further figure out the underlying mechanisms of improved radioresistance by *Bach2* deletion, RNA sequencing (RNA-seq) was performed on crypt samples isolated from the small intestine of KO and control mice (Figures 7A and S6A). As a transcription regulator, the knockdown of *Bach2* levels could consequently affect the expression of many target genes, including those regulating DNA DSB repair and cell cycle (*Cdk6*, *parp1*, *Trp53bp1*, *Msh2*). Moreover, MAplot (Figure S6B) ob-

tained from the RNA-seq dataset shows that the expression of *Parp1*, *Ddb2*, *Ung*, *Mlh1*, and *Msh2* was increased in *Bach2*-deficient crypt cells compared with *Bach2* WT (control) crypt cells. In addition, examination of the promoter regions of potential target genes suggests that *Parp1* and *Ung* genes might have BACH2 binding sites (Figure S6D), and the expression of *Parp1* and *Ung* may be directly regulated by BACH2 binding. Consistently, gene set enrichment analysis (GSEA) also demonstrated significant upregulation of genes in several DNA repair pathways, such as mismatch repair, homologous recombination, base excision repair, and nucleotide excision repair (Figure 7B).

Upon IR, mammalian cells generate enormous DNA DSBs, which are the main cause of mitotic cell death. In response to DSBs, cells undergo mitotic arrest and immediately activate the DNA repair mechanism to ensure genomic integrity. DNA repair efficiency can be evaluated by examining the rate of resolution of  $\gamma$ -H2AX IR-induced repair foci. The resolution of  $\gamma$ -H2AX in ISC or TA cells

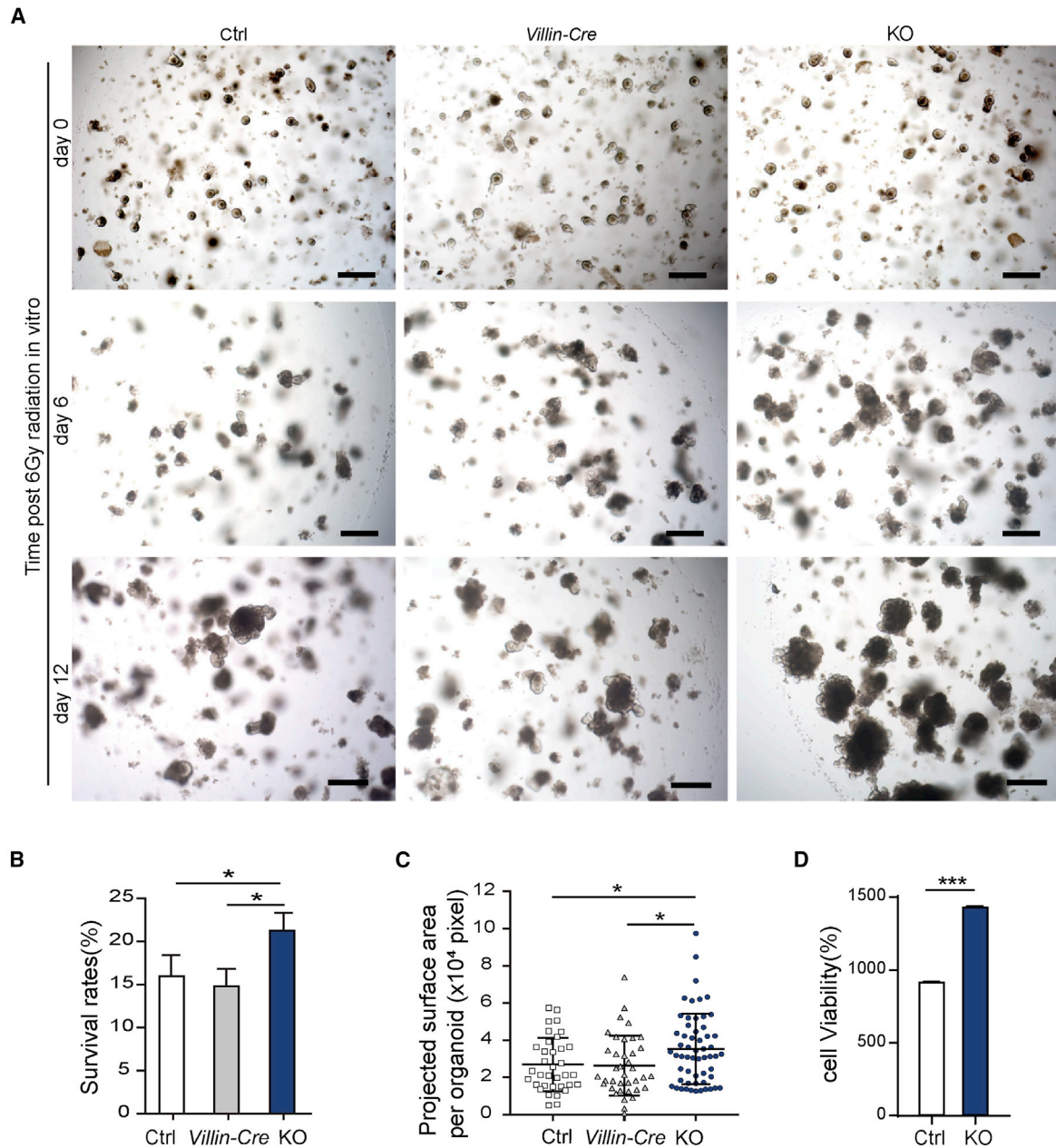


**Figure 5. *Bach2* Ablation Promotes Organoid Survival in 3D Cultures after Irradiation**

(A) Representative images of surviving organoids from *Bach2*-KO, *Bach2*-floxed control (Ctrl), and *Villin-Cre* mice before (day 0) and after 6 Gy radiation. Scale bars, 200  $\mu$ m.

(B) Percentage survival of organoids at day 12 after 6 Gy radiation ( $n > 300$  organoids per group).

(C) Organoid projected surface area ( $n > 35$  organoids per group).

(D) Quantitative analysis of organoid cell viability ( $n = 3$  independent experiments).

Error bars, SD. \* $p < 0.05$ , \*\*\* $p < 0.001$ .

post IR was evaluated by immunofluorescence studies. Our study showed that the  $\gamma$ -H2AX foci were resolved much faster in ISCs from *Bach2*-KO mice than in controls (Figure 7C). Of note, the same phenomenon could also be

observed in TA cells (Figure S7A). Moreover, to provide more support for efficient DNA repair in crypt cells in the absence of *Bach2*, we performed 53BP1 immunofluorescent staining. Consistent with  $\gamma$ -H2AX foci data, the

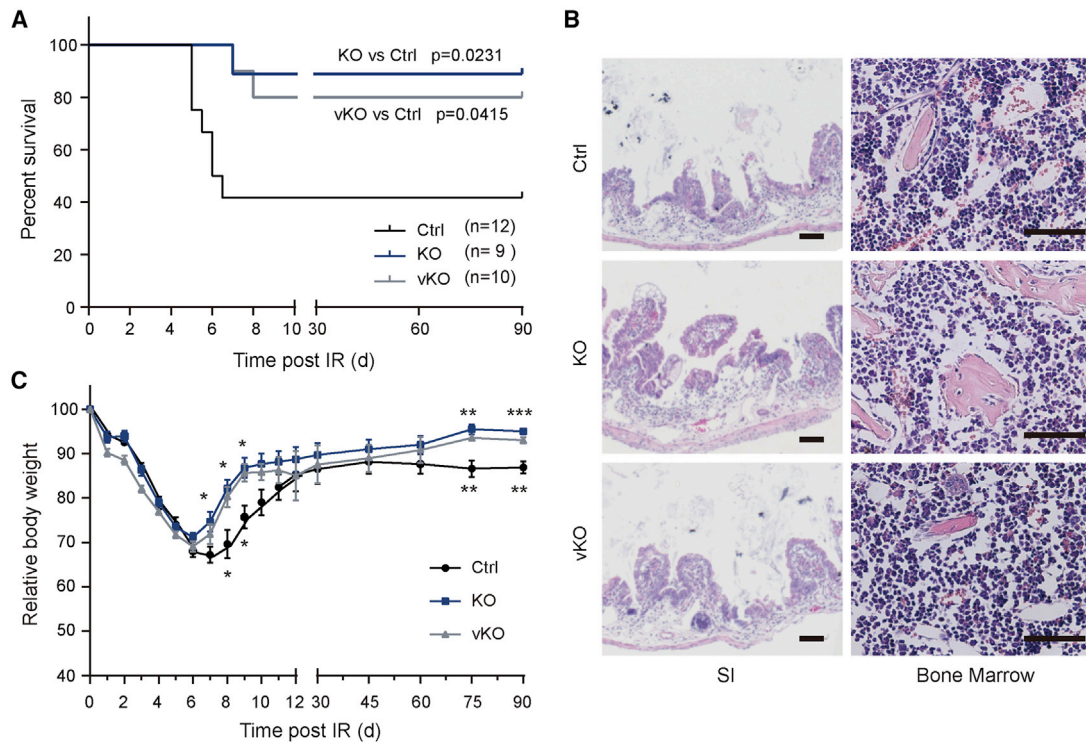


**Figure 6. *Bach2* Deletion Protects Mice from Radiation-Induced Mortality**

(A) Kaplan-Meier survival analysis of *Bach2*-KO, vKO, and control mice after 14 Gy of SBI (KO versus control,  $p = 0.0231$ ; vKO versus control,  $p = 0.0415$ , by log rank test).

(B) H&E-stained sections of proximal jejunum and humerus were obtained from animals displaying an agonal breathing pattern. Murine small intestinal (SI) mucosa was denuded in mice dying after 14 Gy X-ray irradiation, with disrupted villus/crypt structure, although bone marrow was well preserved. Scale bar, 50  $\mu\text{m}$ .

(C) Temporal changes in body weight post irradiation. Error bars, SD. \* $p < 0.05$ , \*\* $p < 0.01$ , \*\*\* $p < 0.001$ .

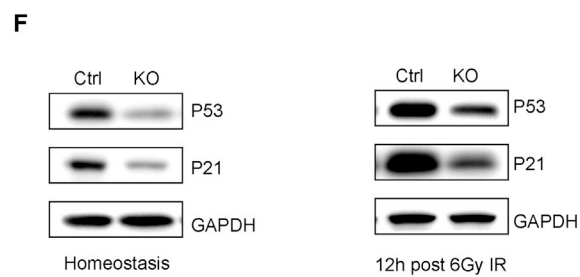
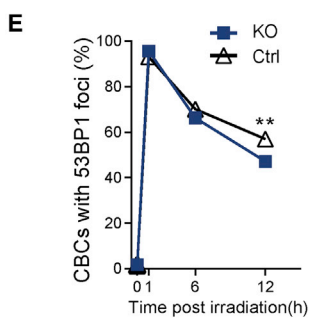
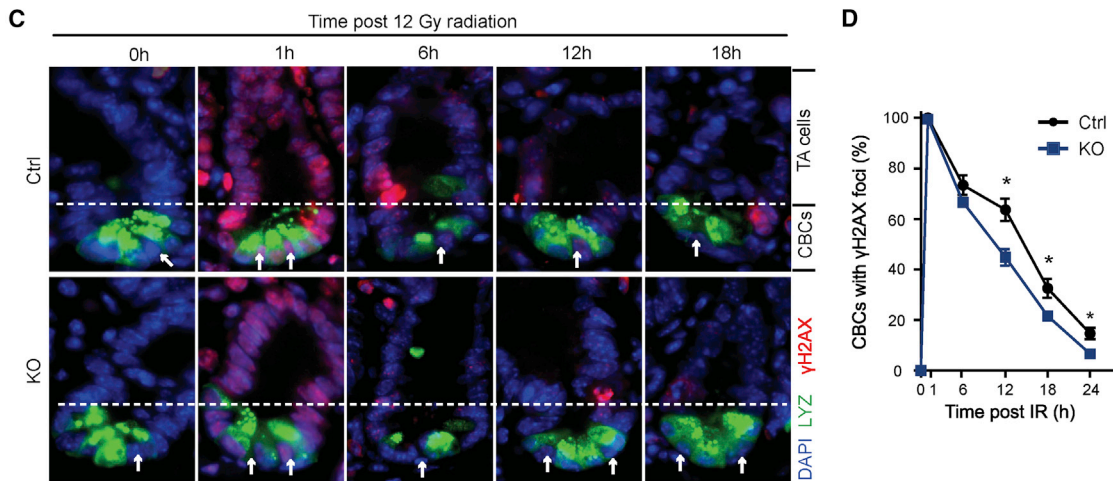
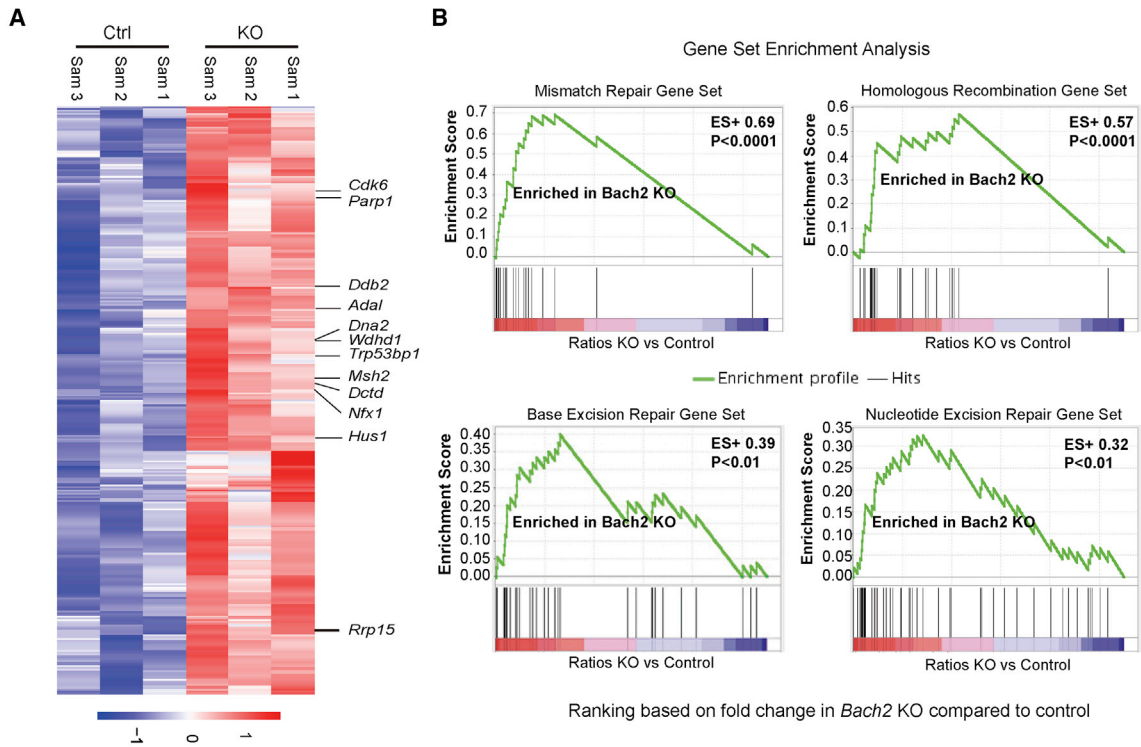
53BP1 immunofluorescent staining (Figures 7E and S7B) showed that ISCs resolve 53BP1 foci more quickly, resulting in a statistical difference in the number of cells displaying detectable 53BP1 foci by 12 h post irradiation (Figure 7E).

Normally, radiation induces DNA DSBs and rapidly activates the G1/S checkpoint via P53-dependent mechanisms. It has been reported that the protein level of P53 is significantly reduced in the absence of *Bach2*, and strongly increased after inducible overexpression of *Bach2* in pre-B cells (Srividya et al., 2013). To investigate the deficiency of *Bach2* in the expression of *p53* in GI epithelial cells, we collected intestinal organoids from *Bach2*-KO and control mice to detect the P53 protein levels with and without irradiation by western blot analysis. Our data show that the protein levels of P53 were significantly decreased in *Bach2*-KO organoids compared with control cells (Figure 7F). Moreover, following 6 Gy irradiation, the P53 protein levels were still significantly lower in *Bach2*-KO cells than in control cells (Figure 7F). Likewise, the protein level of the *p53*-dependent target gene P21 was reduced in the absence

of *Bach2* during homeostasis and after radiation. These data indicated that *Bach2* deficiency may cause a reduction in P53 level, subsequently affecting the cell-cycle checkpoint and progression after radiation.

## DISCUSSION

*Bach2* is a newly discovered transcription factor and plays an important role in normal B cell development and progression of inflammatory disease (Muto et al., 1998; Roychoudhuri et al., 2013; Srividya et al., 2013). Most current studies focus on the role of *Bach2* in regulating immunity, and little is known as to whether *Bach2* could directly regulate intestinal regeneration. High-dose radiation exposure induces GI stem cell death, resulting in denudation of the intestinal mucosa and mortality from the GI syndrome (Burdelya et al., 2008; David G et al., 2010; Qiu et al., 2008). ISCs play a major role in intestinal regeneration after injury. Due to the profound need for efficient intestine function, pathways or genes through which intestinal



(legend on next page)



regeneration can be expedited could dramatically help overall survival.

The *CreER<sup>T2</sup>* or *Villin-CreER<sup>T2</sup>* mice are widely used in genetic studies, although a transient and reversible Cre-mediated genotoxicity in the gut has been reported recently (Bohin et al., 2018). Off-target DNA damage at cryptic *loxP* sites in CreER activation can further affect ISC sensitivity or regeneration ability in response to genome toxicity. Importantly, Bohin et al. found that stem cell impairment is short lived, with return to normal by 7 days post Tam treatment. Our study confirmed the impairment and its normalization in *Villin-CreER<sup>T2</sup>* mice by crypt microcolony assay. When intestinal radiation damage is postponed for 9–10 days after the final Tam injection, the number of regenerated crypts returns to the level of WT, indicating that CreER toxicity can be avoided by taking this “delayed” procedure.

Following the “delayed” method, we found that genetic ablation of *Bach2* in mice resulted in hypertrophic crypts in small intestines of mice (Figures 1 and 2), which is consistent with a previous report that showed that *Bach2*-KO mice developed a progressive wasting disease, resulting in diminished survival compared with control littermates (Roychoudhuri et al., 2013). Furthermore, it also has been reported that silencing of *Bach2* stimulates proliferation and increases cell survival in response to acute oxidative stress, yet its silencing did not protect cells from UV-genotoxic stress (Uittenboogaard et al., 2013). In our study, *Bach2*-deficient mice exhibited a faster crypt regeneration after IR (Figures 3–5), and regenerated crypts in *Bach2*-deficient mice were much larger in size and in quantity, indicating that surviving TA cells might coordinate with ISCs in reconstructing intestinal epithelium. Considering the obvious and significant regeneration phenotype, we tested mouse survival following a lethal dose of radiation. Our data show that *Bach2* ablation did rescue mice from radiation-induced GI syndrome (Figure 6). Thus, *Bach2* is an important regulator of cell proliferation and survival in ISCs and TA cells after IR damage.

The maintenance of genomic integrity following DNA damage depends on the coordination of the DNA repair

system and cell-cycle checkpoint controls. Our data suggest that *Bach2* deficiency stimulates intestinal regeneration by upregulating genes that are critical for DNA DSBs (such as *Parp1*, *Ddb2*, *Ung*, *Mlh1*, and *Msh2*). We found that both ISCs and TA cells from *Bach2*-KO mice repaired DSBs more efficiently than *Bach2*-floxed controls. Kruglov et al. reported that *Parp1* inhibition increased the expression of *Irf8* and *Bcl6*, leading to upregulation of *Blimp1* and *Bax* and subsequently restraining DNA repair in cutaneous T cell lymphoma (Kruglov et al., 2020). Another study reported that *Bcl6* directly regulates *Bach2* expression and *Ung* expression (Alinikula et al., 2011). Interestingly, our MAplot data (Figure S6B) show that the expression of *Parp1*, *Ddb2*, *Ung*, *Mlh1*, and *Msh2* was increased in *Bach2*-deficient crypt cells compared with *Bach2* WT (control) crypt cells. These data may shed light on the network between *Bach2*, *Parp1*, and *Ung*.

Also, intestinal crypt regeneration is required for efficient reconstitution of the normal crypt-villus structure after radiation injury. Efficient DNA repair and quick resumption of the cell cycle play a key role during intestinal regeneration, which is mainly regulated by the *p53* pathway and its transcriptional target *p21*. Our data show that the protein levels of P53 and P21 were significantly decreased in *Bach2*-KO intestinal organoids compared with control during homeostasis and after radiation. These data indicated that *Bach2* deficiency may cause a reduction in P53 level, subsequently resulting in checkpoint failure, accelerating cell-cycle progression and promoting crypt regeneration, which is also consistent with the previous study (Srividya et al., 2013).

In summary, this study shows *Bach2* deficiency promotes intestinal epithelial cell proliferation during homeostasis and induces intestinal regeneration after radiation by upregulation of DNA repair activity and accelerating cell-cycle progression. Therefore, small-molecule compounds capable of inhibiting *Bach2* expression or promoting *Bach2* protein degradation could provide a useful therapeutic strategy for radiation-induced intestinal injury associated with delayed intestinal regeneration and repair.

### Figure 7. *Bach2* Deficiency Facilitates DNA Repair in CBCs after Radiation

(A) Heatmap of crypts isolated from control and *Bach2*-KO mice showing the top 345 upregulated genes. Labeled genes are examples known to be involved in DNA repair (n = 3 mice).

(B) Examples of molecular pathways involved in DNA repair found enriched by GSEA of RNA-seq data. Fold change in gene expression in *Bach2*-KO and control crypt cells is compared. Enrichment score (ES) and p value are shown.

(C) Representative images of  $\gamma$ -H2AX immunofluorescence staining (red) on small intestinal sections from *Bach2<sup>flox/flox</sup>; CreER<sup>T2</sup>* (KO) and control mice (Ctrl) after 12 Gy irradiation. CBCs (white arrows) are interspersed between Paneth cells stained green for lysozyme. Scale bar, 20  $\mu$ m.

(D and E) Kinetic analysis of  $\gamma$ -H2AX (E) and 53BP1 (F) focus resolution in CBCs. Data (mean  $\pm$  SD) were collected from three experiments analyzing 30 CBCs/mouse and two mice/experiment (\*p < 0.05, \*\*p < 0.001).

(F) Western blot analysis of P53 and P21 in organoids derived from *Bach2*-KO and WT (Ctrl) mice during homeostasis (left) and at 12 h post 6Gy irradiation (right) (n = 3 independent experiments).



## EXPERIMENTAL PROCEDURES

### Mouse Models

*Villin-CreER<sup>T2</sup>* mice were kind gifts from Dr. Robine's group (Institut Curie-CNRS, Paris, France). *Bach2<sup>fl/fl</sup>; CreER<sup>T2</sup>* mice were obtained by crossing *Bach2<sup>fl/fl</sup>* mice with *CreER<sup>T2</sup>* mice. *Bach2<sup>fl/fl</sup>; Villin-CreER<sup>T2</sup>* mice were obtained by crossing *Bach2<sup>fl/fl</sup>* with *Villin-CreER<sup>T2</sup>* mice. All mice were maintained on a C57BL/6 genetic background. At least three mice per genotype ranging from 6 to 8 weeks of age were used. For Cre induction, mice were intraperitoneally injected with Tam (Sigma-Aldrich) in corn oil (Sigma-Aldrich) at 80 mg/kg body weight for 5 consecutive days. All animal studies were performed in accordance with the relevant guidelines and under the approval of the Institutional Animal Care and Use Committee of Fudan University.

### Subtotal Body Irradiation

Ten days after Tam administration, mice were treated 50 cm from the radiation source-skin distance (SSD) with 250 kVp X-rays at a dose rate of 246 cGy/min (produced by an X-Rad 320 biological irradiator with 0.25 mm Cu filtration). Briefly, mice were placed into plastic close-fitting jigs, which were covered by a 5 mm thick lead shield from chest and above, leaving the whole of the mouse abdomen exposed to irradiation. After irradiation, the mice were kept in individually ventilated cages until further processing. Mice exposed to a high dose of radiation were given an appropriate liquid diet due to mass disruptions in the intestinal tract.

### Survival of Mice after Irradiation and Evaluation of Cause of Animal Death

Actuarial survival of animals was calculated by the product-limit Kaplan-Meier method. Cause of death was evaluated by autopsy, performed within 60 min of animal death or when terminally sick animals showed an agonal breathing pattern as previous reported (Hua et al., 2012). GI damage was diagnosed as cause of death when the small intestines showed denuded mucosa with nearly no villi or crypts apparent. Bone marrow damage was diagnosed as cause of death when the marrow showed extensive matrix necrosis, widespread hemorrhage, and complete depletion of hematopoietic elements.

### Histopathology Analysis

Tissues were obtained within 60 min after animal death or when terminally sick animals showed an agonal breathing pattern. Intestinal tissues were fixed in freshly prepared 4% neutral buffered paraformaldehyde for 12–16 h and then placed in 70% ethanol until further processing. Bone samples were decalcified in an EDTA glycerol solution for 2 weeks at 4°C. Paraffin embedding and H&E staining were performed as described in the [Supplemental Information](#). GI tract damage was diagnosed as the cause of animal death when the small intestines showed denuded mucosa with nearly absent villus/crypt structures, with intact or proliferative bone marrow. The circumference of a transverse cross section of the intestines was used as a unit and the size was calculated using Image-Pro Plus software (Media Cybernetics).

### Crypts Microcolony Assay

The microcolony assay was performed as previously described (Booth et al., 2012). Briefly, at 3.5 days after irradiation, the small intestines were obtained, formalin fixed overnight, and placed in 70% ethanol. After standard tissue processing, pieces of intestine were embedded in paraffin blocks. Transverse sections of the full intestinal circumference were prepared and stained with H&E. Surviving crypts were defined as containing 10 or more adjacent chromophilic cells and a lumen (Hu et al., 2016). The circumference of a transverse cross section of the intestines was used as a unit. The number of surviving crypts was counted per circumference using a Zeiss microscope.

### $\gamma$ -H2AX and 53BP1 Immunofluorescence

IR and tissue processing were performed as described above. Paraffin-embedded tissue sections were dewaxed, rehydrated, and stained with antibodies using standard procedures. Primary antibody for immunofluorescence was mouse monoclonal anti-H2AX Ser139 (Millipore, 05-636, 1:100), rabbit anti-53BP1 (Novus, NB100-304SS, 1:1,000), and polyclonal goat anti-LYSOZYME (Santa Cruz, sc-27958, 1:1,000). Multichannel fluorescence images were acquired using an upright wide-field Zeiss Imager.M2 microscope.

### Crypt Isolation, Organoid Culture, and Tam Induction

Mouse small intestinal crypts were isolated and cultured as previously described (Sato et al., 2009). Briefly, a fragment (5 cm) of the small intestine was cut longitudinally and washed with cold PBS. The fragment was cut into 5 mm pieces and incubated in cold PBS containing 5 mM EDTA for 40 min. Isolated crypts were enriched and embedded in Matrigel (Corning, 356231) and seeded on 24-well plate. Organoid culture medium was added and refreshed every 2 days. Culture medium contained advanced DMEM/F12 medium (Gibco, 12634-034) supplemented with penicillin/streptomycin (Gibco, 15140-122), 10 mM HEPES (Gibco, 15630-080), 2 mM GlutaMAX (Gibco, 35050-068), 1× N2 (Gibco, 17502-048), 1× B27 (Gibco, 17504-044), 1 mM N-acetylcysteine (Sigma-Aldrich, A9165), 50 ng/mL EGF (Sino Biological, 50482-MNCH), 100 ng/mL Noggin (Sino Biological, 50688-M02H), and 500 ng/mL R-spondin1 (Sino Biological, 11083-HNAS). Organoids were monitored and imaged under microscopy (Zeiss, Vert.A1). The number and size of surviving organoids were calculated using Image-Pro Plus software (Media Cybernetics).

For *in vitro* CreER activation and/or *Bach2* ablation, organoids derived from *Bach2<sup>fl/fl</sup>; CreER<sup>T2</sup>* mice, *Bach2<sup>fl/fl</sup>*; *Villin-CreER<sup>T2</sup>* mice, or *Villin-CreER<sup>T2</sup>* mice were stimulated with 100 nM 4-hydroxytamoxifen (Sigma-Aldrich, SML1666) for 16 h before further processing.

### Organoid Irradiation Response Assays

Organoid size assays were performed as previously described (Yao et al., 2020). Briefly, organoid size was used as the metric for the cellular viability/response. Organoids were photographed every 3 days after irradiation (Zeiss, Vert.A1). The sizes of the live organoids were measured using Image-Pro Plus 6.0 (Media Cybernetics). For dose-response assays, the number of live organoids after



irradiation was counted using ImageJ software (National Institutes of Health, USA), and the organoid survival rate (the number of live organoids on day 6 after irradiation/the number of live organoids on day 0 after irradiation) was calculated. Organoid cell viability was also evaluated every 3 days after irradiation using the Cell-Titer-Glo 3D Cell viability assay (Promega, G9683) according to the manufacturer's instruction.

### RNA-Seq

Crypts were isolated from the small intestines of *Bach2*-KO and control mice ( $n = 3$ , respectively) 10 days after Tam administration. Total RNA was extracted for sequencing using RNA-seq. RNA degradation and contamination were monitored on 1% agarose gels. RNA purity was checked using the NanoPhotometer spectrophotometer (Implen, Westlake Village, CA, USA). A total amount of 3  $\mu\text{g}$  RNA per sample was used as input material for the RNA sample preparations. Sequencing libraries were generated using NEBNext (NEB, USA) following the manufacturer's recommendations, and index codes were added to attribute sequencing to each sample. The clustering of the index-coded samples was performed on a cBot Cluster Generation System using the TruSeq PE Cluster Kit v.3-cBot-HS (Illumina) according to the manufacturer's instructions. After clustering generation, the RNA library preparations were sequenced on an Illumina Hi-seq platform and 125 bp/150 bp paired-end reads were generated.

### Real-Time Quantitative PCR

The total RNA from tissues or organoids was extracted using the RNeasy Mini Kit (Qiagen, 74104) and reverse transcribed to cDNA using the PrimeScript Master Mix (Perfect Real Time) kit (Takara, RR036A), according to the manufacturers' instructions. Real-time qPCR was performed on an Mx3000P real-time PCR system (Stratagene, USA) using the SYBR Premix Ex Taq II (Tli RNaseH Plus) kit (Takara, RR820A). Full details are in the [Supplementary Experimental Procedures](#).

### Statistical Analysis

Data represent the mean  $\pm$  SD. When normality could be assumed, differences were analyzed by two-tailed Student's *t* test; otherwise the Mann-Whitney test was chosen. Kaplan-Meier survival analysis and log rank comparison were performed for survival studies. Statistical analysis was performed with GraphPad Prism6 software. A *p* value of  $\leq 0.05$  was considered significant.

### DATA AND CODE AVAILABILITY

The RNA-seq data have been deposited in ArrayExpression (<https://www.ebi.ac.uk/arrayexpress/>) and are accessible through the accession number (E-MTAB-9865) or through the URL: <https://www.ebi.ac.uk/arrayexpress/experiments/E-MTAB-9865>. Additional data and materials and associated protocols are available upon request from the corresponding authors (G. Hua and J. Gao) to comply with institutional ethics regulations.

### SUPPLEMENTAL INFORMATION

Supplemental Information can be found online at <https://doi.org/10.1016/j.stemcr.2020.12.005>.

### AUTHOR CONTRIBUTIONS

Conception and Design, Y.L., J.G., and G.H.; Development of Methodology, Y.L., X.R., S.C., P.T., Q.G., M.P., G.F., L.L., Y.Y., Z.Z., X.X., and G.H.; Acquisition of Data, Y.L., X.R., S.C., P.T., Q.G., G.F., M.P., and X.G.; Analysis and Interpretation of Data, Y.L., W.H., X.X., J.G., and G.H.; Writing, Review, and/or Revision of the Manuscript, Y.L., J.G., and G.H.; Administrative, Technical, or Material Support, L.L., X.G., and Y.Z.; Supervision, J.G. and G.H.

### ACKNOWLEDGMENTS

We would like to thank Dr. Song Baoliang (Wuhan University, Wuhan, China) and Dr. Robine Sylvie (Institut Curie-CNRS, Paris, France) for sharing *Villin-CreER<sup>T2</sup>* mice. This work was supported by grants from the National Natural Science Foundation of China (31470826 and 31670858 to G.H.). All the authors declare no potential conflicts of interest.

Received: April 29, 2019

Revised: December 2, 2020

Accepted: December 2, 2020

Published: December 30, 2020

### REFERENCES

- Akihiko, M., Satoshi, T., Haruka, T., Akihiro, K., Masamoto, K., Etsuro, I., Masayuki, Y., and Kazuhiko, I. (2014). Activation of Maf/AP-1 repressor *Bach2* by oxidative stress promotes apoptosis and its interaction with promyelocytic leukemia nuclear bodies. *J. Biol. Chem.* *277*, 20724–20733.
- Alinikula, J., Nera, K.P., Junntila, S., and Lassila, O. (2011). Alternate pathways for *Bcl6*-mediated regulation of B cell to plasma cell differentiation. *Eur. J. Immunol.* *41*, 2404–2413.
- Barker, N., van Es, J.H., Kuipers, J., Kujala, P., van den Born, M., Cozijnsen, M., Haegebarth, A., Korving, J., Begthel, H., Peters, P.J., et al. (2007). Identification of stem cells in small intestine and colon by marker gene *Lgr5*. *Nature* *449*, 1003–1007.
- Bjerknes, M., and Cheng, H. (1999). Clonal analysis of mouse intestinal epithelial progenitors. *Gastroenterology* *116*, 7–14.
- Bohin, N., Carlson, E.A., and Samuelson, L.C. (2018). Genome toxicity and impaired stem cell function after conditional activation of *CreER(T2)* in the intestine. *Stem Cell Rep.* *11*, 1337–1346.
- Booth, C., Tudor, G., Tudor, J., Katz, B.P., and MacVittie, T.J. (2012). Acute gastrointestinal syndrome in high-dose irradiated mice. *Health Phys.* *103*, 383–399.
- Burdelya, L.G., Krivokrysenko, V.I., Tallant, T.C., Strom, E., Gleiberman, A.S., Gupta, D., Kurnasov, O.V., Fort, F.L., Osterman, A.L., DiDonato, J.A., et al. (2008). An agonist of toll-like receptor 5 has radioprotective activity in mouse and primate models. *Science* *320*, 226–230.
- David G, K., Philip M, S., Emmanuelle, d.T., Julie, M.S., Wu-Shiun, H., Talya, D., Laura B, J., Pooja, S., Kim, L.M., and Rhianna, C.



- (2010). p53 controls radiation-induced gastrointestinal syndrome in mice independent of apoptosis. *Science* 327, 593–596.
- Hoshino, H., Kobayashi, A., Yoshida, M., Kudo, N., Oyake, T., Motohashi, H., Hayashi, N., Yamamoto, M., and Igarashi, K. (2000). Oxidative stress abolishes leptomycin B-sensitive nuclear export of transcription repressor Bach2 that counteracts activation of Maf recognition element. *J. Biol. Chem.* 275, 15370–15376.
- Hu, B., Jin, C., Li, H.-B., Tong, J., Ouyang, X., Cetinbas, N.M., Zhu, S., Strowig, T., Lam, F.C., Zhao, C., et al. (2016). The DNA-sensing AIM2 inflammasome controls radiation-induced cell death and tissue injury. *Science* 354, 765–768.
- Hua, G., Tin Htwe, T., Regina, F., Adriana, H.F., Hans, C., Zvi, F., and Richard, K. (2012). Crypt base columnar stem cells in small intestines of mice are radioresistant. *Gastroenterology* 143, 1266–1276.
- Kruglov, O., Wu, X., Hwang, S.T., and Akilov, O.E. (2020). The synergistic proapoptotic effect of PARP-1 and HDAC inhibition in cutaneous T-cell lymphoma is mediated via Blimp-1. *Blood Adv.* 4, 4788–4797.
- Mason, K.A., Withers, H.R., McBride, W.H., Davis, C.A., and Smathers, J.B. (1989). Comparison of the gastrointestinal syndrome after total-body or total-abdominal irradiation. *Radiat. Res.* 117, 480–488.
- Muto, A., Hoshino, H., Madisen, L., Yanai, N., Obinata, M., Karasuyama, H., Hayashi, N., Nakauchi, H., Yamamoto, M., Groudine, M., et al. (1998). Identification of Bach2 as a B-cell-specific partner for small Maf proteins that negatively regulate the immunoglobulin heavy chain gene 3' enhancer. *EMBO J.* 17, 5734–5743.
- Oyake, T., Itoh, K., Motohashi, H., Hayashi, N., Hoshino, H., Nishizawa, M., Yamamoto, M., and Igarashi, K. (1996). Bach proteins belong to a novel family of BTB-basic leucine zipper transcription factors that interact with MafK and regulate transcription through the NF-E2 site. *Mol. Cell Biol.* 16, 6083–6095.
- Panagiota A, S., Aurélie, C., Guilhem, M., Sarah, D.C., Khalil Kass, Y., Gaelle, L., Ellen, D., Claudio, S., Geertrui, D., and Jean-Christophe, M. (2010). Bcl-2 and accelerated DNA repair mediates resistance of hair follicle bulge stem cells to DNA-damage-induced cell death. *Nat. Cell Biol.* 12, 572–582.
- Qiu, W., Carson-Walter, E.B., Liu, H., Epperly, M., Greenberger, J.S., Zambetti, G.P., Zhang, L., and Yu, J. (2008). PUMA regulates intestinal progenitor cell radiosensitivity and gastrointestinal syndrome. *Cell Stem Cell* 2, 576–583.
- Roychoudhuri, R., Hirahara, K., Mousavi, K., Clever, D., Klebanoff, C.A., Bonelli, M., Sciumè, G., Zare, H., Vahedi, G., Dema, B., et al. (2013). BACH2 represses effector programs to stabilize Treg-mediated immune homeostasis. *Nature* 498, 506–510.
- Sato, T., Vries, R.G., Snippert, H.J., van de Wetering, M., Barker, N., Stange, D.E., van Es, J.H., Abo, A., Kujala, P., Peters, P.J., et al. (2009). Single Lgr5 stem cells build crypt-villus structures in vitro without a mesenchymal niche. *Nature* 459, 262–265.
- Schwank, G., and Clevers, H. (2016). CRISPR/Cas9-Mediated genome editing of mouse small intestinal organoids. *Methods Mol. Biol.* 1422, 3–11.
- Singh, V.K., Ducey, E.J., Brown, D.S., and Whitnall, M.H. (2012). A review of radiation countermeasure work ongoing at the Armed Forces Radiobiology Research Institute. *Int. J. Radiat. Biol.* 88, 296–310.
- Srividya, S., Chuanxin, H., Huimin, G., Zhengshan, C., Richard, H., Huining, K., Carina, N., Björn, T., Christian, H., and Mohammed Firas, S. (2013). BACH2 mediates negative selection and p53-dependent tumor suppression at the pre-B cell receptor checkpoint. *Nat. Med.* 19, 1014–1022.
- Terry, N.H.A., and Travis, E.L. (1989). The influence of bone marrow depletion on intestinal radiation damage. *Int. J. Radiat. Oncol. Biol. Phys.* 17, 569–573.
- Uittenboogaard, L.M., Payan-Gomez, C., Pothof, J., van Ijcken, W., Mastroberardino, P.G., van der Pluijm, I., Hoeijmakers, J.H.J., and Tresini, M. (2013). BACH2: a marker of DNA damage and ageing. *DNA Repair* 12, 982–992.
- Vitale, I., Manic, G., De Maria, R., Kroemer, G., and Galluzzi, L. (2017). DNA damage in stem cells. *Mol. Cell* 66, 306–319.
- Waselenko, J.K., MacVittie, T.J., Blakely, W.F., Pesik, N., Wiley, A.L., Dickerson, W.E., Tsu, M.H., Confer, D.L., Coleman, C.N., Seed, T., et al. (2004). Medical management of the acute radiation syndrome: recommendations of the strategic national stockpile radiation working group. *Ann. Intern. Med.* 140, 1037–1051.
- Yao, Y., Xu, X., Yang, L., Zhu, J., Wan, J., Shen, L., Xia, F., Fu, G., Deng, Y., Pan, M., et al. (2020). Patient-derived organoids predict chemoradiation responses of locally advanced rectal cancer. *Cell Stem Cell* 26, 17–26.e16.